RSC Advances

PAPER

View Article Online
View Journal | View Issue

Check for updates

Cite this: *RSC Adv.*, 2022, **12**, 33229

Extraction of alumina from high-alumina fly ash by ammonium sulfate: roasting kinetics and mechanism

Xiaoying Li,[a] Bo Hu,[bc] Nengsheng Liu,*[a] Xueqing Liu,[bc] Chengwei Liu,[c] Xintao He[c] and Sufang He[bc]

Received 21st October 2022
Accepted 14th November 2022

DOI: 10.1039/d2ra06658k

rsc.li/rsc-advances

The recycling of aluminum is commonly an important step to achieve the high value-added utilization of fly ash, which is a kind of solid waste generated from coal-fired power plants. In this study, high-alumina fly ash was efficiently activated by ammonium sulfate method and the alumina was efficiently extracted. The effects of roasting temperature, roasting time, and ammonium sulfate/high-alumina fly ash mass ratio on the leaching rate of alumina were fully analyzed, and the roasting kinetics and reaction mechanism in the roasting process were discussed. The experimental results showed that the leaching rate of alumina in the roasted material achieved 93.57% with the roasting temperature of 673 K, the roasting time of 60 min, and the mass ratio of ammonium sulfate to high-alumina fly ash of 6 : 1. The roasting kinetics showed that the reaction between high-alumina fly ash and ammonium sulfate was controlled by internal diffusion, the apparent activation energy was 37.40 kJ mol^{-1}, which accorded with the reaction kinetic equation $1 - 2x/3 - (1 - x)^{2/3} = 2.9546\exp[-37\,400/(RT)]t$. The reaction mechanism showed that the aluminum and structural damage mullite in the high-alumina fly ash reacted with molten ammonium sulfate to form $(NH_4)_3Al(SO_4)_3$ and $NH_4Al(SO_4)_2$. Finally, $(NH_4)_3Al(SO_4)_3$ was transformed into $NH_4Al(SO_4)_2$ with the increase of temperature.

Open Access Article. Published on 21 November 2022. Downloaded on 2/20/2026 11:52:49 PM.
This article is licensed under a Creative Commons Attribution-NonCommercial 3.0 Unported Licence.

1. Introduction

Fly ash, generated from coal-fired power plants,[1,2] is the largest kind of industrial solid waste in China.[3–5] At present, the annual emissions of fly ash in China is 600–800 million tons,[6–8] which is expected to reach 925 million tons in 2024.[9] However, the utilization rate of fly ash is only 25%,[10] resulting in the accumulation of more than 3 billion tons of fly ash.[11] The long-term and large-scale accumulation of fly ash not only causes environmental pollution,[12–14] but also has great harm to crop and human body, so the various treatments have been explored to improve this problem, involving architecture, agriculture, materials, metallurgy, environment and other fields. In order to utilize fly ash and reduce its damage, it is necessary to convert it into high value-added products,[15] which has attracted widespread attention in soil remediation, ceramic material preparation, synthetic catalysts, zeolite preparation, valuable metal recovery and other fields.[16–18]

It is worth mentioning in particular that there is a special kind of fly ash, which comes from Shanxi and the middle and west of Inner Mongolia with the abundant aluminum content up to 40–60%,[19] called high-alumina fly ash.[20,21] Due to the aluminum content in high-alumina fly ash is comparable to a medium grade bauxite, so it can be used as a potential raw material to replace bauxite and recover alumina, alleviate the shortage of bauxite resources in China, and reduce the environmental pollution caused by fly ash accumulation.[19] However, aluminum in high-alumina fly ash mainly exists in the form of stable mullite, leading to the difficulty for the direct extraction of aluminum.[22] Therefore, the key to the utilization of high-alumina fly ash is to destroy the structure of mullite through activation.

There are many methods about fly ash activation, such as acid method, alkali method, thermal activation by calcination, sodium hydrogen sulfate roasting method,[23] thermal activation by potassium bisulfate,[24] potassium pyrosulfate calcination activation method,[19] *etc.* The traditional and effective activation method of high-alumina fly ash is alkali fusion method, which means that high-alumina fly ash is mixed with solid alkali such as NaOH, KOH, $NaCO_3$, Na_2SO_4 or K_2SiO_3 (ref. 5) evenly and roasted at high temperature to achieve the purpose of activation.[25,26] However, the process of alkali fusion is usually high cost, high temperature, high energy consumption and low activation efficiency.[27] Therefore, in terms of environment and

[a]*Faculty of Metallurgical and Energy Engineering, Kunming University of Science and Technology, Kunming 650093, China. E-mail: liunengshengms@163.com*
[b]*Research Center for Analysis and Measurement, Kunming University of Science and Technology, Kunming 650093, China*
[c]*Faculty of Materials Science and Engineering, Kunming University of Science and Technology, Kunming 650093, China*

© 2022 The Author(s). Published by the Royal Society of Chemistry

Open Access Article. Published on 21 November 2022. Downloaded on 2/20/2026 11:52:49 PM.
This article is licensed under a Creative Commons Attribution-NonCommercial 3.0 Unported Licence.

economy, it is necessary to find a new activator to further reduce energy consumption.

Ammonium sulfate method is a newly developed activation technology in recent years,[28,29] which can produce alumina products with high purity and has high commercial value. Especially, the activation process of ammonium sulfate, with low cost and recyclable tail gas, does not involve strong acid, strong alkali or strong corrosive agent and is less corrosive to the equipment, so there is a broad industrial application prospect with its unique advantages.[30,31] Briefly speaking, the ammonium sulfate method involves the reaction of ammonium sulfate with high alumina fly ash in the temperature range of 300–400 °C to produce soluble aluminum sulfate, which converts mullite, an inert component of high alumina fly ash, into silica and soluble aluminum salts, thus facilitating the extraction of aluminum and silica elements and the preparation of silica materials.[31] For instance, Li *et al.*[31] conducted three times recrystallization of ammonium aluminum sulfate solutions obtained by this method to obtain high-purity alumina with a purity of more than 99.9%. Park[32] extracted high concentration alumina from fly ash by ammonium sulfate low-temperature sintering method, the extraction rate of aluminum can reach 94.36%. Li[33] studied the process of extracting alumina from fly ash by ammonium sulfate, and the recovery rate was 95.6%. Frederic J. Doucet *et al.*[34] studied the feasibility of recovering aluminum from ammonium sulfate and found that 95% of aluminum could be recovered at 1 h, 500 °C, with a 2 : 6 weight ratio of fly ash to ammonium sulfate. Their results indicated that ammonium sulfate method was a good activation method and the study of it was very necessary.

At present, most researches on ammonium sulfate activation of high-alumina fly ash were mainly focused on the optimization of experimental process parameters to efficiently extract alumina, the in-depth studies on roasting kinetics and reaction mechanism in the roasting process, which is important to the efficient activation and comprehensive utilization of high-alumina fly ash, have been less addressed. Therefore, in order to promote further development of alumina extraction from high-alumina fly ash *via* the ammonium sulfate method, this method was first used to treat the raw material high-alumina fly ash from a power plant in Inner Mongolia, China. On the basis of studying the effect of process parameters on the extraction rate of alumina from high-alumina fly ash, the thermodynamics and kinetics, as well as associated factors in roasting process were examined, and the reaction mechanism was deduced. This study aims to reveal the reaction mechanism of ammonium sulfate activation high-alumina fly ash, optimize the roasting parameters and kinetic parameters, and provide certain theoretical guidance for the efficient activation and comprehensive utilization of high-alumina fly ash.

2. Experimental

2.1. Raw materials and reagents

High-alumina fly ash came from a thermal power plant in Inner Mongolia, China; the ammonium sulfate ($(NH_4)_2SO_4$) and the sulfuric acid (H_2SO_4) used in the experiment were analytically pure and obtained from Tianjin Ruijinte Chemicals Co., Ltd, China; and the water used in the experiment was distilled water.

2.2. Experimental method

First, the high-alumina fly ash and ammonium sulfate were mixed evenly with a certain mass ratio in the crucible, and then heated in a muffle furnace at a heating rate of 10 °C min^{-1}. When the set temperature was reached, the timing device was started immediately.[35] After sintering, the sample was cooled, grinded, weighed and characterized. Subsequently, this sample was transferred to the beaker and leached by sulfuric acid of 10% (with the liquid–solid ratio of 10 : 1) at 90 °C for 1 h, followed by vacuum filtration, washing, and drying. Finally, the Al^{3+} content in the filtrate was determined by Inductively coupled plasma-optical emission spectrometer, and afterwards the aluminum leaching rate (η), which can be used as the evaluation basis for the activation effect of high-alumina fly ash, was calculated using $\eta = (V_cC_x)/(MW_x) \times 100\%$.[36] Where M (g) is the quantity of raw high-alumina fly ash material, W_x (wt%) is the mass fraction of aluminum in the raw high-alumina fly ash material, C_x (g L^{-1}) is the mass concentration of Al^{3+} ions in the acid leaching solution, and V_c (L) is the volume of the prepared acid leaching solution.[4]

2.3. Sample characterization

The elemental analysis of raw material was carried out by X-ray fluorescence (XRF, XRF-1800, Shimadzu, Kyoto, Japan, instrument working voltage 40 kV, working current 95 mA, prt 8 mL min^{-1}). The crystalline phases and surface morphology of raw material and important solid roasted material were examined and scanned by X-ray diffraction (XRD, TTRAX III, Japan, Cu-Kα radiation, tube current 700 mA, tube voltage 40 kV, step sizes 0.2°, scanning range 2θ = 5°–90°, scanning rate 10° min^{-1}), scanning electron microscopy (SEM, Nova Nano-SEM 450, FEI, USA, acceleration voltage: 50 V to 30 kV, magnification 20–1000k). The aluminum content in aluminum liquid was determined by an inductively coupled plasma-optical emission spectrometer (ICP-OES, ICAP7400 Radial, Thermo Scientific, USA). The carbon contents analysis was performed *via* an infrared carbon and sulfur analyzer (CS 2000, ELTRA, Germany). The particle size distribution was measured using Rise-2002 laser particle size analyzer (Jinan Runzhi Technology Co., Ltd.).

3. Results and discussion

3.1. Characterization of raw high-alumina fly ash

In order to obtain the phase transformation and chemical reactions of high-alumina fly ash and ammonium sulfate in the roasting process, the raw material of high-alumina fly ash was first characterized by XRF, XRD and SEM to understand its chemical compositions, phase compositions and appearance morphology.

The chemical compositions (mass fraction) of raw fly ash were measured by XRF and infrared carbon and sulfur analyzer, and the results were presented in Table 1. The main

© 2022 The Author(s). Published by the Royal Society of Chemistry

Open Access Article. Published on 21 November 2022. Downloaded on 2/20/2026 11:52:49 PM.
This article is licensed under a Creative Commons Attribution-NonCommercial 3.0 Unported Licence.

Table 1 Chemical compositions of high-alumina fly ash in Inner Mongolia (wt%)

Component	SiO_2	Al_2O_3	Fe_2O_3	CaO	TiO_2	C
Content/wt%	37.40	46.22	3.05	5.17	3.51	2.54

components were SiO_2 and Al_2O_3, with the contents were 37.40% and 46.22%, respectively. Obviously, it is a kind of high-alumina fly ash. As well, there were a little amount of Fe_2O_3 (3.05%), CaO (5.17%), TiO_2 (3.51%) and C (2.54%) in this sample.

In addition, the phase compositions of raw high-alumina fly ash were studied by XRD and the results were shown in Fig. 1(A). According to PDF#10-0173, PDF#46, PDF#15-0076 and previous literature,[30,37,38] the diffraction peaks at 16.44°, 23.99°, 25.99°, 31.40°, 33.16°, 37.37°, 39.39°, 40.80°, 42.43°, 54.01°, 60.74°, 62.55°, 64.70°, 70.95°, 74.94°, 84.87° and 88.65° were assigned to mullite ($Al_6Si_2O_{13}$); while the peaks at 19.72°, 26.60°, 36.08°, 39.39°, 45.66°, 50.10°, 54.96°, 67.12° and 81.85° were corresponded to amorphous SiO_2; in addition, Al_2O_3 phase could be also found at peaks of 25.42°, 35.53°, 43.33°, 52.23°, and 57.48°. The particle size distribution of high alumina fly ash in Fig. 1(B) showed that the maximum particle size was 30 μm, and more than 98% of the material diameter was distributed in the range of 0–60 μm, and the material size was relatively fine. The surface morphology of high-alumina fly ash was characterized by SEM,

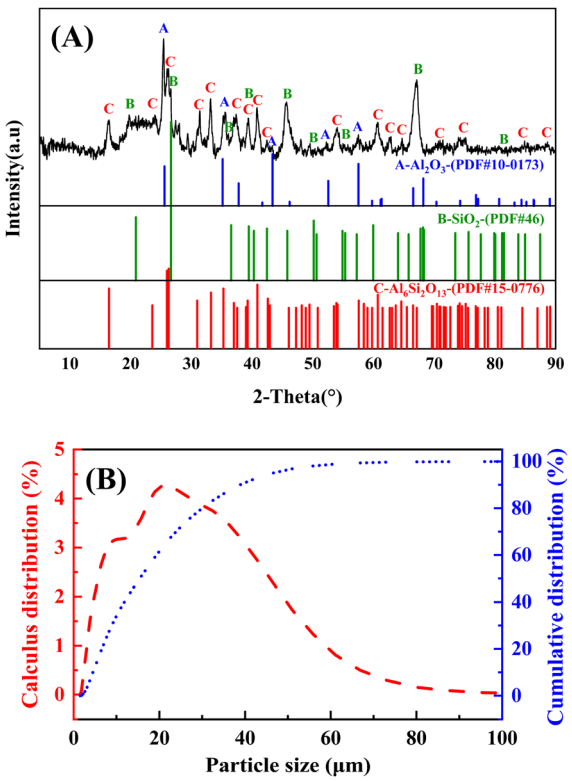

Fig. 1 (A) XRD pattern and (B) particle size distribution of raw high-alumina fly ash.

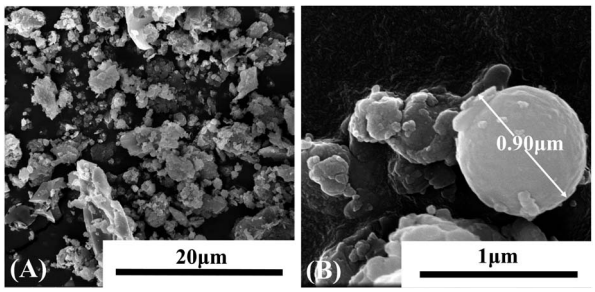

Fig. 2 SEM image of raw high-alumina fly ash. (A) Low magnification image and (B) high magnification image.

as shown in Fig. 2. Fig. 2(A) was obtained at 8k magnification, it can be seen that high-alumina fly ash was composed of a large number of spherical, spherical particles, and rod-like particles.[30] Fig. 2(B) was shot at the magnification of 150k, which further showed that the spherical particles in Fig. 2(A) were smooth and dense. It had a stable structure with a particle size of about 0.9 μm.

3.2. Optimization of roasting parameters

For the roasting procedure, the alumina extraction efficiency was significantly influenced by several operational parameters such as the roasting temperature, roasting time and mass ratio of ammonium sulfate to high-alumina fly ash. In order to balance the roasting efficiency and cost, optimize the roasting parameters and discover the roasting kinetics of ammonium sulfate and high-alumina fly ash, the optimization of the roasting conditions was necessary. Therefore, the law of change of aluminum extraction rate under different roasting conditions was investigated, as shown in Fig. 3.

3.2.1. Effect of roasting temperature. The influence of roasting temperature (573, 593, 613, 633, 653, 673, 693 K) on the leaching rate of aluminum was presented in Fig. 3(A). Obviously, in the temperature range of 573–673 K, the aluminum leaching rate was greatly improved with the increase of roasting temperature, and the aluminum leaching rate increased from 49.00% to 93.57%. However, when the temperature reached 693 K, there was a decrease in the aluminum leaching rate to 90.14% in relation to ammonium sulfate/high-alumina fly ash mass ratio (and any further rise in temperature affects aluminum leaching[39]). It may be due to the fact that with the increase of roasting temperature, the decomposition of ammonium salt became more intense, resulting in the volatilization of ammonia, sulfur oxide, and other gases, so that the effective material ratio of ammonium sulfate to high-alumina fly ash was decreased, which cannot meet the ammonium salt required for the decomposition of high-alumina fly ash, and thus affected the activation of high-alumina fly ash. In addition, excessive temperatures greatly increased the amount of energy used, 673 K was found to be the optimum roasting temperature for high-alumina fly ash activation.[3]

3.2.2. Effect of roasting time. The effect of the roasting time (5, 10, 20, 40, 60, 90, 120 min) on the leaching rate of aluminum was investigated at the roasting temperature of 673 K

© 2022 The Author(s). Published by the Royal Society of Chemistry

Open Access Article. Published on 21 November 2022. Downloaded on 2/20/2026 11:52:49 PM.
This article is licensed under a Creative Commons Attribution-NonCommercial 3.0 Unported Licence.

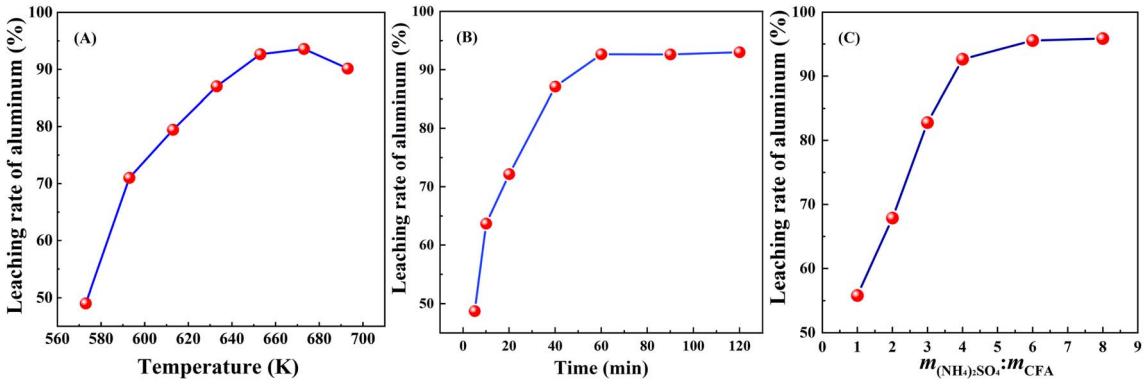

Fig. 3 Effect of roasting temperature (A), roasting time (B), mass ratio of ammonium sulfate to high-alumina fly ash (C) on the leaching rate of aluminum. Experimental conditions: (A) roasting time = 60 min, mass ratio of ammonium sulfate to high-alumina fly ash = 6 : 1; (B) roasting temperature = 673 K, mass ratio of ammonium sulfate to high-alumina fly ash = 6 : 1; (C) roasting temperature = 673 K, roasting time = 60 min.

and the mass ratio of ammonium sulfate to high alumina fly ash of 6 : 1. As evident from Fig. 3(B), the leaching rate of aluminum increased rapidly when the roasting time was extended from 5 min to 60 min before reaching a plateau. With a roasting time of 5 min, the leaching rate of aluminum was only 48.73% because the time employed was too short to facilitate the reaction between high-alumina fly ash and ammonium sulfate.[3] It was found that the leaching rate of aluminum was over 93% when the roasting time was 60 min. However, with a further extension of the roasting time, there was little improvement in the leaching rate of aluminum, which indicates that 60 min is adequate for activating the high-alumina fly ash. Any longer not only increased the amount of energy consumed, but also increased the process time involved and affected process efficiency.[3] Therefore, 60 min was set as the optimal roasting time.

3.2.3. Effect of mass ratio of ammonium sulfate to high-alumina fly ash. Moreover, ammonium sulfate was an activator of high-alumina fly ash, and the amount of ammonium sulfate had a direct impact on its activation effect. To determine the effect of mass ratio of ammonium sulfate to high-alumina fly ash (1 : 1, 2 : 1, 3 : 1, 4 : 1, 6 : 1, 8 : 1) on the leaching rate of aluminum, experiments were performed with roasting temperature 673 K and roasting time 60 min, and the results were shown in Fig. 3(C). When the mass ratio of ammonium sulfate to high-alumina fly ash was 1 : 1, the leaching rate of aluminum was 55.83%, which indicated that there was insufficient ammonium sulfate to react all the mullite in the high-alumina fly ash.[3] The leaching rate of aluminum increased with an increase in the mass ratio of ammonium sulfate to high-alumina fly ash: when the mass ratio of ammonium sulfate to high-alumina fly ash was 6 : 1, the leaching rate of aluminum reached 93.57%, which showed that high-alumina fly ash can be fully activated by ammonium sulfate under this condition.[3] However, with a further increase in the amount of ammonium sulfate added, there was little improvement in the leaching rate of aluminum, and the higher mass ratio was found to have little effect on high-alumina fly ash activation. For example, when the mass ratio of ammonium sulfate to high-alumina fly ash was 8 : 1, the leaching rate of aluminum reached 93.88%, which was only 0.31% higher than that when the mass ratio was 6 : 1, leading to an increase in acid consumption and energy consumption in the subsequent acid leaching process. The results indicated that the maximum economic benefit was provided when the ammonium sulfate/high alumina fly ash mass ratio was 6 : 1.

As mentioned previously, the optimum roasting conditions for using ammonium sulfate to roast and activate high-alumina fly ash were as follows: the roasting temperature was 673 K, the roasting time was 60 min, and mass ratio of ammonium sulfate to high-alumina fly ash was 6 : 1. Under these conditions, the leaching rate of aluminum reached 93.57%. According to previous literature (Table 2),[30,40,41] the leaching rate of aluminum in this study was higher than most of them, which evidenced that this study was essential. It can be seen from the Fig. 3 that the roasting temperature had a great influence on the extraction rate of aluminum. Next, the roasting kinetics was discussed.

3.3. Roasting kinetics analysis

3.3.1. Kinetics under different roasting conditions. When the mass ratio of ammonium sulfate to high-alumina fly ash

Table 2 The leaching rate of aluminum in previous literature[30,40,41]

Author	Temperature	Ratio of ammonium sulfate to high-alumina fly ash	Time	Leaching rate of aluminum
Yan Wu[30]	653 K	6 : 1	120 min	82.00%
Yusheng Wu[40]	673 K	—	180 min	85.00%
Liyan Sun[41]	713 K	4.5 : 1	40 min	90.00%
This study	673 K	6 : 1	60 min	93.57%

© 2022 The Author(s). Published by the Royal Society of Chemistry

Open Access Article. Published on 21 November 2022. Downloaded on 2/20/2026 11:52:49 PM.
This article is licensed under a Creative Commons Attribution-NonCommercial 3.0 Unported Licence.

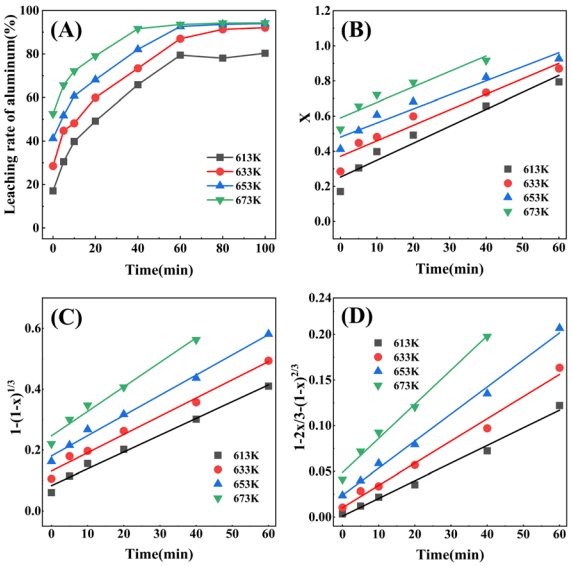

Fig. 4 (A) Leaching rate of aluminum at different roasting conditions, relationship between different kinetic models (B) $F_1(x) = x$, (C) $F_2(x) = 1 - (1-x)^{1/3}$, (D) $F_3(x) = 1 - 2x/3 - (1-x)^{2/3}$ and reaction time at different roasting temperatures. Experimental conditions: mass ratio of ammonium sulfate to high-alumina fly ash = 6 : 1.

was 6 : 1 and the leaching conditions were the same, the effects of roasting temperature and roasting time on roasting process were studied at 613 K, 633 K, 653 K, and 673 K roasting for 0 min, 5 min, 10 min, 20 min, 40 min, 60 min, 80 min, 100 min respectively, and the results were shown in Fig. 4(A). It can be seen that the leaching rate of aluminum increased with the increase of roasting temperature and roasting time, especially the former one affected more significantly. It is worth emphasizing that the extraction rate of aluminum at 0 min was not 0, due to the fact that there was a period of temperature rise before the set temperature was reached, during which the reaction had already occurred, so the extraction rate was not 0.[35] In addition, the change of aluminum leaching rate was divided into two stages. In the former stage, with the extension of roasting time, the aluminum leaching rate continued to increase under different temperature conditions; in the latter stage, the aluminum leaching rate of each temperature curve tended to be stable with the extension of time. Considering comprehensively, in the roasting temperature range of 613–673 K, the roasting time range of kinetic fitting was 0–60 min for 613–653 K, and the roasting time range of kinetic fitting was 0–40 min for 673 K.

3.3.2. Kinetic model. According to the nature of the materials, the melting point of ammonium sulfate was 553 K, which was lower than the experimental temperature during roasting, the activator ammonium sulfate was melted into liquid at 613–673 K. Therefore, the roasting activation reaction of high aluminum fly ash with ammonium sulfate as an additive belonged to the liquid–solid reaction process. The process of liquid–solid reaction was generally that the liquid reactant reached the surface of the solid particle through the liquid boundary layer, then diffused from the particle surface to the reaction interface, followed by the chemical reaction between the liquid reactants and solid reactants in contact with each other, the products diffused from the reaction interface to the particle surface, and finally the products diffused from the particle surface to the liquid boundary layer. In order to better understand the mechanism in the oxidation roasting process, roasting kinetic analysis was used to define the chemical behaviors in the thermal reaction process.[42–44] Table 3 listed three kinetic equations of external diffusion, internal diffusion and chemical reaction in the oxidation roasting process, which can summarize the whole liquid–solid reaction process.[45,46]

Table 3 Kinetic equations in the oxidation roasting[a]

Equations	Equations: $g(x) = k(T)t$	Reaction mechanisms
$F_1(x)$	$x = k_1 t$	External diffusion
$F_2(x)$	$1 - (1-x)^{1/3} = k_2 t$	Chemical reaction
$F_3(x)$	$1 - 2x/3 - (1-x)^{2/3} = k_3 t$	Internal diffusion

[a] Where x is the extraction rate of aluminum; k is the apparent rate constant; t is the reaction time.

3.3.3. Apparent activation energy and kinetic equation. It can be seen from Table 3 that the solid–liquid reaction in the roasting process may be controlled by internal diffusion, external diffusion or chemical reaction. In order to determine the specific control step, the data in Fig. 4(A) were substituted into Table 3, and the results were shown in Fig. 4(B)–(D). The values of R^2 were obtained by fitting the kinetic equations $F(x)$, which revealed the different reaction mechanisms. The fitting results were shown in Table 4. By comparing the linear regression coefficient (R^2) of various kinetic models, the mathematical expression of the specific $g(x)$ function was determined.[47] In Table 4, the R^2 of $F_3(x)$ at 613 K, 633 K and 653 K corresponded to 0.99108, 0.98720 and 0.99476 respectively in the previous stage of 0–60 min, and the R^2 of $F_3(x)$ at 673 K was 0.99109 in the previous stage of 0–40 min. It was found that the R^2 value of $F_3(x)$ was closer to 1 than other roasting kinetic models, indicating that the roasting activation process of high alumina fly ash–ammonium sulfate system was controlled by internal diffusion.

The simulated data of the most probably roasting kinetics were shown in Fig. 4(D). The apparent reaction rate constant k was obtained by calculating the slope of the reaction models, the values of R^2 were obtained by linear fitting, and the values of k and R^2 were shown in Table 5. It can be seen from Table 5 that the apparent reaction rate constant k increased from 0.00193 to 0.00374 when the thermodynamic temperature was increased from 613 K to 673 K, indicating that the thermodynamic temperature had a great influence on apparent reaction rate

Table 4 Linear regression coefficient (R^2) of different kinetic models

Time/min^{-1}	Temperature/K	$F_1(x)$	$F_2(x)$	$F_3(x)$
0–60	613	0.95048	0.98879	0.99108
0–60	633	0.94293	0.98608	0.98720
0–60	653	0.94477	0.99281	0.99476
0–40	673	0.90794	0.98026	0.99109

© 2022 The Author(s). Published by the Royal Society of Chemistry

Open Access Article. Published on 21 November 2022. Downloaded on 2/20/2026 11:52:49 PM.
This article is licensed under a Creative Commons Attribution-NonCommercial 3.0 Unported Licence.

Table 5 The apparent reaction rate constant and the linear correlation coefficient at different temperatures

Temperature (K)	Apparent reaction rate constant k (s^{-1})	Linear correlation coefficient R^2
613	0.00193	0.99108
633	0.00243	0.98720
653	0.00296	0.99476
673	0.00374	0.99109

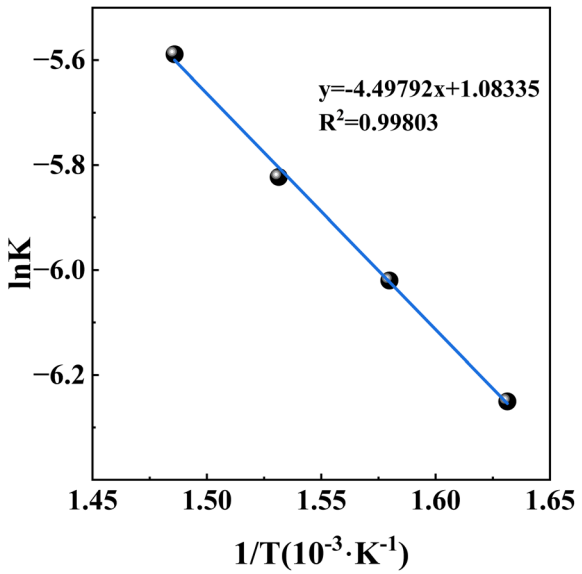

Fig. 5 Relationship between $\ln k$ and T^{-1} (k is the apparent reaction rate constant, T is the thermodynamic temperature).

constant, and the increase of the thermodynamic temperature could accelerate apparent reaction rate constant.

According to the Arrhenius formula $\ln k = \ln A - E_a/RT$ (where k is the rate constant; A is the frequency factor; E_a is the apparent activation energy, J mol^{-1}; R is the mole gas constant (8.314 J mol^{-1} K^{-1}) and T is the thermodynamic temperature), $\ln k$ was used to regress T^{-1} to explore the relationship between chemical reaction rate constant and temperature, and the results were shown in Fig. 5. It was very obvious that $\ln k$ had a better linear relationship with T^{-1} (the R^2 is close to 1 with a value of 0.99803). Combining $\ln k = \ln A - E_a/RT$ with $y = -4.49792x + 1.08335$ in Fig. 5, the values of apparent activation energy E_a and A were obtained with 37.40 kJ mol^{-1} and 2.9546, respectively. There were some differences compared to the literature,[31] which was normal because of different raw materials, different chemical reagents and different chemical reactions. Bringing the experimental data into $1 - 2x/3 - (1 - x)^{2/3} = kt$, the kinetic equation of high-alumina fly ash–ammonium sulfate system in the roasting activation process was obtained: $1 - 2x/3 - (1 - x)^{2/3} = 2.9546 \exp[-37\,400/(RT)]t$.

3.4. Reaction mechanism

In order to further deduce the reaction mechanism of roasting process, the activated materials under different roasting conditions were characterized and analyzed by thermodynamics.

The possible chemical reactions in the roasting process are listed below:[48,49]

$$6(NH_4)_2SO_4 + Al_2O_3 = 2(NH_4)_3Al(SO_4)_3 + 6NH_3\uparrow + 3H_2O\uparrow \quad (1)$$

$$18(NH_4)_2SO_4 + Al_6Si_2O_{13} = 6(NH_4)_3Al(SO_4)_3 + 18NH_3\uparrow + 9H_2O\uparrow + 2SiO_2\uparrow \quad (2)$$

$$(NH_4)_2SO_4 = NH_4HSO_4 + NH_3\uparrow \quad (3)$$

$$Al_6Si_2O_{13} + 12(NH_4)_2SO_4 = 6NH_4Al(SO_4)_2 + 2SiO_2 + 18NH_3\uparrow + 9H_2O\uparrow \quad (4)$$

$$Al_2O_3 + 4(NH_4)_2SO_4 = 2NH_4Al(SO_4)_2 + 6NH_3\uparrow + 3H_2O\uparrow \quad (5)$$

$$Fe_2O_3 + 3(NH_4)_2SO_4 = Fe_2(SO_4)_3\uparrow + 6NH_3\uparrow + 3H_2O\uparrow \quad (6)$$

$$(NH_4)_2SO_4 = 2NH_3\uparrow + H_2O\uparrow + SO_3\uparrow \quad (7)$$

$$4(NH_4)_3Al(SO_4)_3 + Al_2O_3 = 61NH_4Al(SO_4)_2 + 6NH_3\uparrow + 3H_2O\uparrow \quad (8)$$

$$NH_4HSO_4 = NH_3\uparrow + H_2O\uparrow + SO_3\uparrow \quad (9)$$

By roasting, alumina in high-alumina fly ash can be converted to soluble $(NH_4)_3Al(SO_4)_3$ and $NH_4Al(SO_4)_2$ by the reaction between molten ammonium sulfate and alumina and damaged mullite.

The high-alumina fly ash–ammonium sulfate mixtures were roasted and activated at different temperatures (573–693 K) with the mass ratio of ammonium sulfate to high-alumina fly ash of 6 : 1, roasting time of 60 min. And the phase transformations of the mixtures were investigated by XRD. The XRD comparison charts of the high-alumina fly ash–ammonium sulfate mixtures were shown in Fig. 6, the main XRD peaks for different materials are listed in Table 6.[31,38,50] Obviously, the main phases of

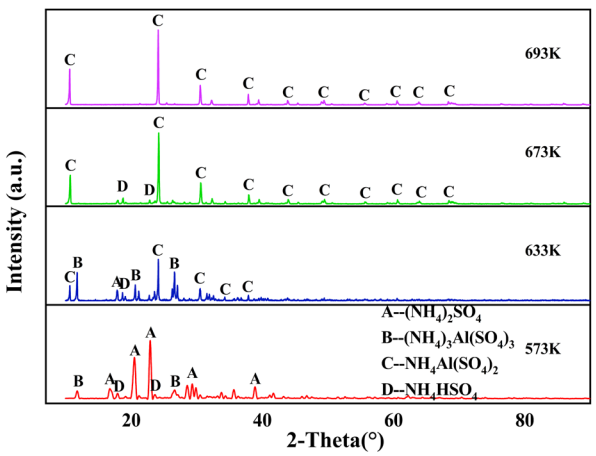

Fig. 6 XRD patterns of high-alumina fly ash–ammonium sulfate mixtures roasted at different temperatures. Experimental conditions: mass ratio of ammonium sulfate to high-alumina fly ash = 6 : 1, roasting time = 60 min.

© 2022 The Author(s). Published by the Royal Society of Chemistry

Open Access Article. Published on 21 November 2022. Downloaded on 2/20/2026 11:52:49 PM. This article is licensed under a Creative Commons Attribution-NonCommercial 3.0 Unported Licence.

Table 6 The main XRD peaks for different materials

Temperature	Main phase	2theta (°)				
573 K	$(NH_4)_2SO_4$	16.76	20.52	22.94	29.32	38.84
	$(NH_4)_3Al(SO_4)_3$	11.78	26.62	—	—	—
	NH_4HSO_4	17.94	23.58	—	—	—
633 K	$(NH_4)_2SO_4$	17.86	—	—	—	—
	$(NH_4)_3Al(SO_4)_3$	11.78	20.62	26.62	—	—
	$NH_4Al(SO_4)_2$	10.64	24.14	30.52	34.28	37.88
	NH_4HSO_4	18.68	—	—	—	—
673 K	$NH_4Al(SO_4)_2$	10.72	24.22	30.62	37.92	43.94
		49.46	55.64	60.64	63.94	68.46
	NH_4HSO_4	18.78	22.84	—	—	—
693 K	$NH_4Al(SO_4)_2$	10.64	24.12	30.54	37.86	43.86
		49.72	55.52	60.56	63.88	68.38

the sample roasted at 573 K were found to be $(NH_4)_2SO_4$ and $(NH_4)_3Al(SO_4)_3$, and there was a small amount of NH_4HSO_4, indicating that the molten ammonium sulfate had reacted with alumina and the damaged mullite to form ammonium aluminum sulfate, so the reactions (1)–(3) were verified.[31] At the same time, the extraction rate of aluminum in the roasted material was 49%, which indicated that the reaction degree was limited. After roasted at 633 K, a new phase –$NH_4Al(SO_4)_2$– were observed in the sample, so the reactions (4) and (5) began to happen under this condition.[31,48,50] Simultaneously, the extraction rate of aluminum in the roasted material was 86.82%, indicating that a large number of aluminum-containing materials in high-alumina fly ash had reacted with ammonium sulfate to form soluble ammonium aluminum sulfate. In addition, the main phases were NH_4HSO_4 and $NH_4Al(SO_4)_2$ in the sample at 673 K. Compared with 633 K, the peaks of NH_4HSO_4 and $NH_4Al(SO_4)_2$ continued to exist and were enhanced, but the characteristic peaks of $(NH_4)_2SO_4$ and $(NH_4)_3Al(SO_4)_3$ disappeared which due to the reactions (1)–(8) were over, respectively.[48,50,51] At this time, the extraction rate of aluminum in the roasted material reached 93.57%, the reaction between high-alumina fly ash and ammonium sulfate was relatively complete, achieving high efficiently activate high-alumina fly ash. As the roasting temperature continued to rise to 693 K, the characteristic peak of NH_4HSO_4 disappeared, the characteristic peak of $NH_4Al(SO_4)_2$ continued to exist, and the extraction rate of aluminum in the roasted material under this condition was 90.14%. Compared to 673 K, the extraction rate was decreased, which may be related to the decomposition of ammonium salt in the raw material and the relatively low mass ratio of ammonium sulfate to high-alumina fly ash in the material,[3] reaction (9) was finished.[48,50,51]

The chemical compositions of the roasted sample and the acid leached residue were measured by XRF and were shown in Table 7. Sample 1 was roasted at a roasting temperature of 673 K, roasting time of 60 min, and a mass ratio of 6 : 1 of ammonium sulfate to high alumina fly ash, and the total amount of elements measured by XRF was 67.5% less than 100%, which was because nitrogen and hydrogen could not be measured. The main elements were S (31.1043%), O (27.0454%), Al (5.0143%), Si (2.3086%), with higher S, O content, which corresponded to the NH_4HSO_4 and $NH_4Al(SO_4)_2$ phases in XRD (Fig. 6 – 673 K). Sample 2 was 0.71 g residue obtained from 10 g sample 1 after acid leaching, the total amount of elements measured by XRF was 85.7%, the main elements were Si (33.6134%), O (44.6783%), Al (6.0732%), the content of Si and O was high, which corresponded to the SiO_2 phase in XRD (Fig. 7), while Al was the percentage of 0.71 g residue, so the amount of residual Al amount was very small and it was calculated that 91.4% of Al was extracted by XRF. Fig. 7 showed the XRD pattern of the residue after roasting with ammonium sulfate high alumina fly ash with a mass ratio of 6 : 1 at 673 K for 60 min and leaching with 10% volume fraction of sulfuric acid at 90 °C for 60 min at a liquid to solid ratio of 10 : 1. Only amorphous silica was detected in the residue, and other substances such as mullite

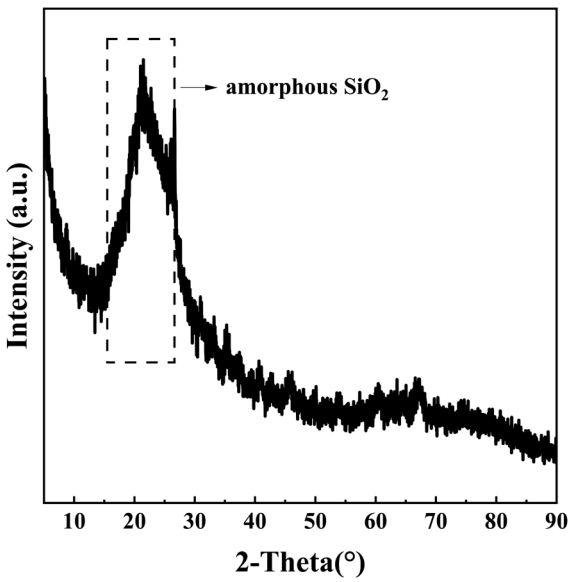

Fig. 7 XRD pattern of residue after leaching by H_2SO_4. Experimental conditions: roasting temperature = 673 K, roasting time = 60 min, mass ratio of ammonium sulfate to high-alumina fly ash = 6 : 1, leaching at 90 °C for 1 h with 10% volume fraction of sulfuric acid at a liquid to solid ratio of 10 : 1.

Table 7 The chemical compositions of the roasted sample 1 and the acid leached residue 2 (wt%) (sample 1 was roasted at a roasting temperature of 673 K, roasting time of 60 min, and a mass ratio of 6 : 1 of ammonium sulfate to high alumina fly ash; sample 2 was 0.71 g residue obtained from 10 g sample 1 after acid leaching)

Sample	O	Al	Si	P	S	K	Ca	Ti	Fe	Zn	Sr	Y	Zr
1	27.0454	5.0143	2.3086	—	31.1043	0.0668	0.7211	0.5349	0.4616	0.1473	0.0334	—	0.0290
2	44.6783	6.0732	33.6134	0.1143	0.2510	0.1227	0.0887	0.4048	0.2348	—	0.0246	0.0046	0.0529

Open Access Article. Published on 21 November 2022. Downloaded on 2/20/2026 11:52:49 PM.
This article is licensed under a Creative Commons Attribution-NonCommercial 3.0 Unported Licence.

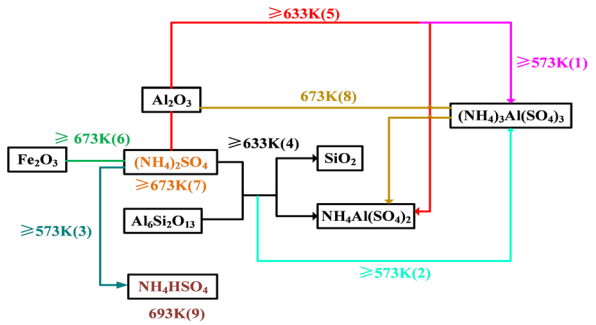

Fig. 8 Phase transformation mechanism of high-alumina fly ash–ammonium sulfate mixtures.

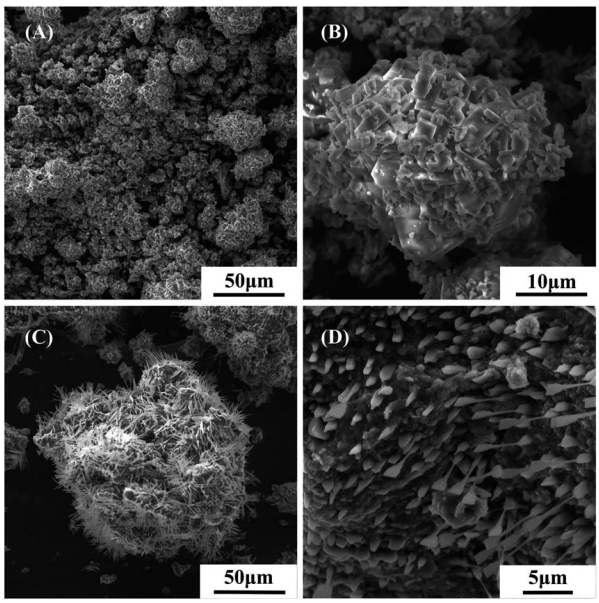

Fig. 9 SEM images of high-alumina fly ash–ammonium sulfate mixtures (A and B) sintered at 573 K for 60 min, (C and D) sintered at 633 K for 60 min. Experimental conditions: mass ratio of ammonium sulfate to high-alumina fly ash = 6 : 1, (A and C) low magnification image and (B and D) high magnification image.

and aluminum-containing compounds were not detected, showing that NH_4HSO_4 and $NH_4Al(SO_4)_2$ generated during roasting were completely dissolved in sulfuric acid solution, and the aluminum in high-alumina fly ash was leached out by the acid, further confirming that high-alumina fly ash can be activated efficiently by ammonium sulfate.

Based on the analysis of XRD patterns, the reaction path of the high-alumina fly ash–ammonium sulfate mixtures under the experimental conditions was obtained, as shown schematically in Fig. 8.

In the condition of the temperatures of 573 K and 633 K, and duration of 60 min, the SEM images of high-alumina fly ash–ammonium sulfate mixtures were shown in Fig. 9. Fig. 9(A) showed that the particle structure of the mixture was similar, and there was agglomeration between particles. Fig. 9(B) showed that the material appearance and morphology further demonstrated this melt aggregation phenomenon, however, the degree of melt aggregation of the material was low. The results confirmed that the mass transfer rate of high-alumina fly ash ammonium sulfate was accelerated and the occurrence of reactions was promoted by melt polymerization at 573 K, the reactions (1)–(3) were confirmed again. Correspondingly, the XRD patterns of the activated materials showed that the main phases of the activated materials were ammonium sulfate and ammonium aluminum sulfate. Fig. 9(C) showed that the outer surface of each particle was similar and whiskers were formed. Fig. 9(D) further confirmed the appearance of crystal morphology. Correspondingly, XRD patterns of activated materials showed that the main phases of activated materials were $(NH_4)_2SO_4$, $(NH_4)_3Al(SO_4)_3$, $NH_4Al(SO_4)_2$ and NH_4HSO_4, indicating that a large number of aluminum-bearing materials in high-alumina fly ash had reacted with ammonium sulfate to form soluble ammonium aluminum sulfate, which confirmed the occurrence of reactions (1)–(5) again.

The above XRD and SEM analysis were complementary and revealed the mechanism of the activation process.

Fig. 10 was the reaction mechanism diagram. It can be seen that at 298 K, the reaction did not occur because the temperature range of roasting activation reaction was not reached. With the increase of temperature, ammonium sulfate reached the

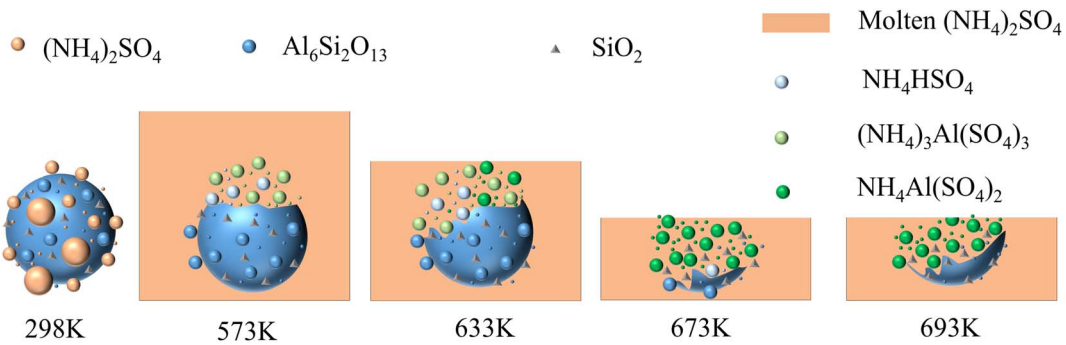

Fig. 10 Mechanism diagram.

© 2022 The Author(s). Published by the Royal Society of Chemistry

Open Access Article. Published on 21 November 2022. Downloaded on 2/20/2026 11:52:49 PM.
This article is licensed under a Creative Commons Attribution-NonCommercial 3.0 Unported Licence.

melting point and became a molten state. At 573 K, the molten ammonium sulfate reacted with the structurally damaged mullite to form $(NH_4)_3Al(SO_4)_3$, coinciding with reactions (1) and (2), and some ammonium sulfate was decomposed into NH_4HSO_4, such as reaction (3). At 633 K, the reactions (1)–(3) were enhanced and a new phase $NH_4Al(SO_4)_2$ was formed, coinciding with reactions (4) and (5). At 673 K, $(NH_4)_2SO_4$ disappeared, indicating that the reactions (1)–(7) were ended. Moreover, $(NH_4)_3Al(SO_4)_3$ had completely disappeared and all transformed into $NH_4Al(SO_4)_2$, reaction (8) was completed. At 693 K, it can be found that only $NH_4Al(SO_4)_2$ was observed, and NH_4HSO_4 was completely disappeared, reaction (9) was over. At the same time, the further decomposition of ammonium salt in the raw material produced ammonia, sulfur trioxide and other gases, which made the effective mass ratio of ammonium sulfate to high-alumina fly ash in the material decrease, and resulted in the whole reaction degree and the leaching rate of aluminum were decreased.

In brief, the amorphous silicon dioxide contained in high-alumina fly ash was unchanged during the whole reaction process, indicating that the reaction of high-alumina fly ash–ammonium sulfate system was mainly the reaction between molten ammonium sulfate and structurally damaged mullite.

4. Conclusions

On the basis of thermodynamic analysis, ammonium sulfate was used as an activator to roast and activate high-alumina fly ash. The effects of roasting process (roasting temperatures, roasting times, mass radio of ammonium sulfate to high-alumina fly ash) on the aluminum extraction were discussed, and the reaction mechanism was investigated through chemical reactions and phase transformation in the roasting process. A summary and main conclusions are as follows:

(1) The main components of high-alumina fly ash were mullite ($Al_6Si_2O_{13}$) and amorphous SiO_2, as well as impurity oxide Fe_2O_3. It was found that temperature had a great influence on the effect of high-alumina fly ash activation. The highest aluminum extraction rate of 93.57% was achieved when ammonium sulfate was roasted with high alumina fly ash at a mass ratio of 6 : 1 at 673 K for 60 min.

(2) The roasting activation process of high alumina fly ash–ammonium sulfate system was a liquid–solid reaction process and controlled by internal diffusion, with an apparent activation energy of 37.40 kJ mol^{-1}. The kinetic equation was: $1 - 2x/3 - (1 - x)^{2/3} = 2.9546 \exp[-37\,400/(RT)]t$.

(3) The phase transformation and morphology of high-alumina fly ash–ammonium sulfate system roasted at different temperatures were thoroughly investigated by XRD and SEM. The alumina and structurally damaged mullite in high-alumina fly ash can react with the molten ammonium sulfate. At 573 K, the ammonium sulfate salt was $(NH_4)_3Al(SO_4)_3$; at 633 K, the ammonium sulfate salts were mainly $(NH_4)_3Al(SO_4)_3$ and $NH_4Al(SO_4)_2$; at 673 K and 693 K, the ammonium sulfate salt was $NH_4Al(SO_4)_2$. In the reaction process, the appearance morphology of the material agglomerated, which enhanced the mass transfer process and promoted the occurrence of reactions.

(4) Based on these investigations and analysis, the reaction mechanism of high-alumina fly ash–ammonium sulfate mixtures was mainly the reaction between molten ammonium sulfate and structurally damaged mullite.

Author contributions

Xiaoying Li performed the experiments and analysis and wrote the main manuscript text. Bo Hu and Xueqing Liu helped Xiaoying Li in analyzing kinetics and mechanism. Xintao He and Chengwei Liu gave some guidance on the means of the analysis of the material. Nengsheng Liu and Sufang He guided the research and revised the draft.

Conflicts of interest

There are no conflicts to declare.

Acknowledgements

The authors are grateful for the financial support provided by the National Natural Science Foundation of China (No. 51704137) and Yunnan Ten Thousand Talents Plan Young & Elite Talents Project (YNWR-QNBJ-2018-067 and YNWR-QNBJ-2020-002).

References

1 S. S. Alterary and N. H. Marei, *J. King Saud Univ., Sci.*, 2021, **33**, 101536.
2 P. Laxmidhar and D. Subhakanta, *Emerging Mater. Res.*, 2020, **9**, 921–934.
3 T. Hu, L. Y. Kou, L. Yang, B. C. Zhou and J. W. Zhou, *Powder Technol.*, 2021, **377**, 739–747.
4 L. Y. Kou, J. W. Zhou, L. Yang, T. Hu and B. C. Zhou, *Mater. Res. Express*, 2020, **7**, 025515.
5 Y. W. Xing, F. Y. Guo, M. D. Xu, X. H. Gui, H. S. Li, G. S. Li, Y. C. Xia and H. S. Han, *Powder Technol.*, 2019, **353**, 372–384.
6 W. Liu, J. W. Liang, C. Fu, B. B. Zeng, M. P. Huang, G. Yang, X. D. Luo, D. An, S. Wei, Z. P. Xie and G. Z. Xu, *Ceram. Int.*, 2022, **48**, 18588–18595.
7 J. J. Yang, H. J. Sun, T. J. Peng, L. Zeng and L. Chao, *Clean Technol. Environ. Policy*, 2022, **24**, 1507–1519.
8 G. Li, M. Li, X. Zhang, P. Cao, H. Jiang, J. Luo and T. Jiang, *Int. J. Min. Sci. Technol.*, 2022, **32**, 563–573.
9 H. Yuan, Y. Yong, C. Wei, W. Shu, Z. Dongmei and Y. Ce, Think Tank Era, 2019, **29**, p. 274.
10 Z. Zimar, D. Robert, A. Zhou, F. Giustozzi, S. Setunge and J. Kodikara, *J. Environ. Manage.*, 2022, **312**, 114926.
11 G. Sun, J. Zhang, B. Hao, X. Li, M. Yan and K. Liu, *Chemosphere*, 2022, **298**, 134136.
12 Y. Liang, S. Chen, J. X. Zhong, H. Ding, Z. L. Zhu and S. Li, *J. Sol-Gel Sci. Technol.*, 2022, **103**, 185–194.
13 V. Gadore and M. Ahmaruzzaman, *J. Water Proc. Eng.*, 2021, **41**, 101910.

Open Access Article. Published on 21 November 2022. Downloaded on 2/20/2026 11:52:49 PM. This article is licensed under a Creative Commons Attribution-NonCommercial 3.0 Unported Licence.

14 E. V. Fomenko, N. N. Anshits, L. A. Solovyov, Y. V. Knyazev, S. V. Semenov, O. A. Bayukov and A. G. Anshits, *ACS Omega*, 2021, **6**, 20076–20085.
15 L. Y. Sun, K. Luo, J. R. Fan and H. L. Lu, *Fuel*, 2017, **199**, 22–27.
16 J. K. Zhang, K. J. Wen and L. Li, *Fuel*, 2021, **286**, 119386.
17 T. Seki, K. Nakamura, Y. Ogawa and C. Inoue, *Environ. Monit. Assess.*, 2021, **193**, 225.
18 D. Langauer, V. Cablik, S. Hredzak, A. Zubrik, M. Matik and Z. Dankova, *Materials*, 2021, **14**, 1267.
19 C. B. Guo, L. Zhao, J. Yang, K. H. Wang and J. J. Zou, *J. Cleaner Prod.*, 2020, **271**, 122703.
20 J. E. Nyarko-Appiah, W. Yu, P. Wei, W. Jiang, Z. Liang and S. Gong, *Fuel*, 2022, **310**, 122434.
21 J. Chen, R. Yang, Z. Zhang and D. Wu, *J. Hazard. Mater.*, 2022, **421**, 126817.
22 G. H. Bai, Y. H. Qiao, B. Shen and S. L. Chen, *Fuel Process. Technol.*, 2011, **92**, 1213–1219.
23 C. B. Guo, J. J. Zou, Y. S. Jiang, T. P. Huang, Y. Cheng and C. D. Wei, *J. Mater. Sci.*, 2014, **49**, 4315–4322.
24 C. Guo, J. Zou, S. Ma, J. Yang and K. Wang, *Minerals*, 2019, **9**, 585.
25 S. Sanchindapong, C. Narattha, M. Piyaworapaiboon, S. Sinthupinyo, P. Chindaprasirt and A. Chaipanich, *J. Therm. Anal. Calorim.*, 2020, **142**, 167–174.
26 J. Cao, P. Wang and Q. Sun, *Z. Anorg. Allg. Chem.*, 2020, **646**, 1666–1670.
27 Z. Cai and Y. Zhang, *RSC Adv.*, 2017, **7**, 36917–36922.
28 J. Ding, S. Ma, S. Shen, Z. Xie, S. Zheng and Y. Zhang, *Waste Manag.*, 2017, **60**, 375–387.
29 D. Valeev, P. Bobylev, N. Osokin, I. Zolotova, I. Rodionov, C. Salazar-Concha and K. Verichev, *J. Cleaner Prod.*, 2022, **363**, 132360.
30 W. Yan, X. Haixia, X. Yujun and L. Jianan, *J. Phys.: Conf. Ser.*, 2019, **1347**, 012111.
31 P. Wang, L. S. Li and D. Z. Wei, *Chin. J. Chem. Eng.*, 2014, **22**, 1027–1032.
32 H. C. Park, Y. J. Park and R. Stevens, *Mater. Sci. Eng., A*, 2004, **367**, 166–170.
33 L. Li, X. Liao, Y. Wu and Y. Liu, *Extracting Alumina from Coal Fly Ash with Ammonium Sulfate Sintering Process*, Orlando, FL, 2012.
34 F. J. Doucet, S. Mohamed, N. Neyt, B. A. Castleman and E. M. van der Merwe, *Hydrometallurgy*, 2016, **166**, 174–184.
35 L.-L. Sui and Y.-C. Zhai, *Trans. Nonferrous Met. Soc. China*, 2014, **24**, 848–853.
36 L. Tao, L. Wang, K. Yang, X. Wang, L. Chen and P. Ning, *RSC Adv.*, 2021, **11**, 5741–5752.
37 B. Zhou, J. Zhou, T. Hu, L. Yang, G. Lin and L. Zhang, *Mater. Res. Express*, 2018, **6**, 015502.
38 R. C. Wang, Y. C. Zhai and Z. Q. Ning, *Int. J. Miner., Metall. Mater.*, 2014, **21**, 144–149.
39 N. Li, J. Guo, Z. Chang, H. Dang, X. Zhao, S. Ali, W. Li, H. Zhou and C. Sun, *RSC Adv.*, 2019, **9**, 23908–23915.
40 Y. S. Wu, P. Xu, J. Chen, L. S. Li and M. C. Li, *Chin. J. Chem. Eng.*, 2014, **22**, 1363–1367.
41 L. Y. Sun, K. Luo, J. R. Fan and H. L. Lu, *Fuel*, 2017, **199**, 22–27.
42 L. Tian, A. Gong, X. G. Wu, J. H. Li, C. W. Liu, X. Q. Yu and Z. F. Xu, *Powder Technol.*, 2020, **373**, 362–368.
43 L. Jie, Y. Li, H. Duan, X. Guo and Y. Zhai, *Russ. J. Non-Ferrous Metals*, 2019, **59**, 596–604.
44 B. Wang, T. Liu, Y. M. Zhang and J. Huang, *Minerals*, 2017, **7**, 43.
45 X. R. Zhu, X. H. Liu and Z. W. Zhao, *Hydrometallurgy*, 2019, **186**, 83–90.
46 J. Ma, Y. Zhang, Y. Qin, Z. Wu, T. Wang and C. Wang, *Ultrason. Sonochem.*, 2017, **35**, 304–312.
47 W. J. Zhang, C. Y. Wang and B. Z. Ma, *Trans. Nonferrous Met. Soc. China*, 2019, **29**, 859–867.
48 G. Q. Zhang, T. Hu, W. J. Liao and X. D. Ma, *J. Environ. Chem. Eng.*, 2021, **9**, 105332.
49 F. Y. Meng, X. S. Li, L. Shi, Y. J. Li, F. Gao and Y. Z. Wei, *Miner. Eng.*, 2020, **157**, 106561.
50 G. S. Li, X. L. Xiong, L. P. Wang, L. Che, L. Z. Wei, H. W. Cheng, X. L. Zou, Q. Xu, Z. F. Zhou, S. G. Li and X. G. Lu, *Metals*, 2019, **9**, 1256.
51 S. Chaudhury, K. D. S. Mudher and V. Venugopal, *J. Nucl. Mater.*, 2003, **322**, 119–125.

© 2022 The Author(s). Published by the Royal Society of Chemistry